Physiol Genomics 50: 332–342, 2018.
First published February 23, 2018; doi:10.1152/physiolgenomics.00133.2017.

RESEARCH ARTICLE | *General Interest*

Na^+/H^+ exchanger isoform 1-induced osteopontin expression facilitates cardiac hypertrophy through p90 ribosomal S6 kinase

Nabeel Abdulrahman,[1] Beatrice Jaspard-Vinassa,[2] Larry Fliegel,[3] Aayesha Jabeen,[1] Sadaf Riaz,[1] Alain-Pierre Gadeau,[2] and Fatima Mraiche[1]

[1]*College of Pharmacy, Qatar University, Doha, Qatar;* [2]*University of Bordeaux, INSERM, Biology of Cardiovascular Disease, U1034, Pessac, France; and* [3]*Department of Biochemistry, Faculty of Medicine and Dentistry, University of Alberta, Edmonton, Alberta, Canada*

Submitted 7 December 2017; accepted in final form 21 February 2018

Abdulrahman N, Jaspard-Vinassa B, Fliegel L, Jabeen A, Riaz S, Gadeau AP, Mraiche F. Na^+/H^+ exchanger isoform 1-induced osteopontin expression facilitates cardiac hypertrophy through p90 ribosomal S6 kinase. *Physiol Genomics* 50: 332–342, 2018. First published February 23, 2018; doi:10.1152/physiolgenomics.00133.2017.—Cardiovascular diseases are the leading cause of death worldwide. One in three cases of heart failure is due to dilated cardiomyopathy. The Na^+/H^+ exchanger isoform 1 (NHE1), a multifunctional protein and the key pH regulator in the heart, has been demonstrated to be increased in this condition. We have previously demonstrated that elevated NHE1 activity induced cardiac hypertrophy in vivo. Furthermore, the overexpression of active NHE1 elicited modulation of gene expression in cardiomyocytes including an upregulation of myocardial osteopontin (OPN) expression. To determine the role of OPN in inducing NHE1-mediated cardiomyocyte hypertrophy, double transgenic mice expressing active NHE1 and OPN knockout were generated and assessed by echocardiography and the cardiac phenotype. Our studies showed that hearts expressing active NHE1 exhibited cardiac remodeling indicated by increased systolic and diastolic left ventricular internal diameter and increased ventricular volume. Moreover, these hearts demonstrated impaired function with decreased fractional shortening and ejection fraction. Atrial natriuretic peptide (ANP) and brain natriuretic peptide (BNP) mRNA was upregulated, and there was an increase in heart cell cross-sectional area confirming the cardiac hypertrophic effect. Moreover, NHE1 transgenic mice also showed increased collagen deposition, upregulation of CD44 and phosphorylation of p90 ribosomal s6 kinase (RSK), effects that were regressed in OPN knockout mice. In conclusion, we developed an interesting comparative model of active NHE1 transgenic mouse lines which express a dilated hypertrophic phenotype expressing CD44 and phosphorylated RSK, effects which were regressed in absence of OPN.

cardiac hypertrophy; Na^+/H^+ exchanger isoform 1; osteopontin; p90 ribosomal s6 kinase

INTRODUCTION

Cardiovascular diseases (CVD) are the leading cause of death globally with an expectation of more than 23.6 million deaths per year by 2030. Mortality due to CVD represented 31% of all global deaths in the year 2013 (42). Cardiac hypertrophy is a type of cardiac remodeling characterized by enlargement of heart and individual myocytes. Cardiac hypertrophy is either due to physiological (pregnancy, exercise) or pathological (hypertension, ischemia) conditions. Cardiac hypertrophy is a compensatory mechanism by the heart to adapt with the hemodynamic load exerted and, if prolonged, may result in heart failure (15, 26, 33).

Na^+/H^+ Exchanger Isoform 1 Induces Cardiac Hypertrophy

Na^+/H^+ exchangers are membrane proteins that function to regulate intracellular pH by extruding intracellular H^+ in exchange of one extracellular Na^+ (6, 24). Previous studies have reported that enhanced activity of Na^+/H^+ exchanger isoform 1 (NHE1), a cardiac-specific form of Na^+/H^+ exchanger family, promotes cardiac hypertrophy (44). Furthermore, inhibition of Na^+/H^+ exchanger activity attenuated the characteristics of isoproterenol induced cardiac hypertrophy in rats (5). Moreover, NHE1 inhibition resulted in glycogen synthase 3-β activation and respective attenuation of hypertrophy in neonatal cardiomyocytes (12). A recent study has reported that specific silencing of myocardial NHE1 with short hairpin RNA is a therapeutic strategy to reduce cardiac hypertrophy (25). Another recent study has demonstrated that an inhibitor of renal sodium glucose transporter (SGLT) 2, empagliflozin, has an effect on regulating intracellular ion homeostasis in cardiomyocytes through direct interaction with Na^+/H^+ exchanger without the involvement of SGLTs (1). Unfortunately, the positive results seen in animal model were not accomplished in clinical trials, where the administration of a NHE1 inhibitor produced serious cerebrovascular side-effects in patients with coronary heart disease (13). Therefore, exploring the signaling pathways downstream of NHE1 promoting cardiac hypertrophy would be highly desirable, resulting in an indirect inhibition of NHE1 and thereby evading the undesired side-effects of NHE1 inhibitors.

Osteopontin Mediates NHE1-induced Cardiac Hypertrophy

It was reported that activated NHE1 protein resulted in an increased activation of osteopontin (OPN) (44), a multifunctional protein that acts as a mediator in various cardiovascular diseases (41) and whose expression is found to be increased in conditions that promote cardiac hypertrophy (10, 43). Furthermore, an increase in OPN expression is seen in a Type 2 diabetes mellitus embryopathy model inducing cardiac fibrosis and hypertrophy (16). Moreover, serum- and glucocorticoid-inducible kinase (sgk1)-mediated cardiac hypertrophy and el-

Address for reprint requests and other correspondence: F. Mraiche, College of Pharmacy, Qatar Univ., PO Box 2713, Doha, Qatar (e-mail: fatima.mraiche@qu.edu.qa).

evated NHE1 expression induced by dexamethasone are accompanied by increased OPN expression (40). Furthermore, it was demonstrated that NHE1-induced cardiac hypertrophy is mediated by OPN through the calcineurin/nuclear factor of activated T cell (NFAT) pathway (22). This infers that OPN is a regulator in NHE1-induced cardiac hypertrophy, and OPN will be a therapeutic target to cardiac hypertrophy. Therefore, experiments were performed on transgenic mice overexpressing NHE1 and OPN knockout overexpressing NHE1 mice to delineate signaling mechanisms by which NHE1 induces OPN expression and thereby contributes to cardiac hypertrophy.

p90 Ribosomal s6 Kinase as a Link between NHE1 and OPN?

Members of mitogen-activated protein kinase (MAPK) pathway including extracellular signal regulated kinase (ERK) and its downstream effectors have been implicated to play significant functions in pathogenesis of cardiac hypertrophy and heart failure (37). Previous research has demonstrated that the ERK pathway of the MAPK cascade activates NHE1 in response to growth factors (2). Moreover, foregoing studies have established that p90 ribosomal s6 kinase (RSK), a downstream mediator of ERK, is a mediator of Na^+/H^+ exchange activity (34, 36).

Therefore, we hypothesize that NHE1-induced cardiac hypertrophy mediated by OPN involves the activation of RSK. To support our hypothesis, characteristics and biomarkers of cardiac hypertrophy, activation of RSK, were analyzed and compared in wild-type (WT) mice, NHE1 overexpressing transgenic mice, OPN knockout NHE1 transgenic mice, and in OPN knockout mice. We found that overexpression of NHE1 induced cardiac hypertrophy manifested by increased ANP and BNP mRNA expression, increased heart cell cross-sectional area, and increased collagen deposition. The collagen deposition was significantly reduced when OPN was knocked out emphasizing the role of OPN in NHE1-induced cardiac hypertrophy. NHE1 overexpression also increased phosphorylation of RSK, which was regressed in the absence of OPN.

MATERIALS AND METHODS

Materials

All routine chemicals were purchased from BD Biosciences (San Jose, CA), Fisher Scientific (Ottawa, ON, Canada), or Sigma (St. Louis, MO). Primary antibodies used for Western blotting included rabbit antibody connexin 43 (c6219, Sigma), rabbit antibody NFAT c4 (13036, Santa Cruz), rabbit antibody phospho-ERK 1/2 (9101, Cell Signaling), rabbit antibody ERK 1/2 (9102, Cell Signaling), rabbit antibody phospho p90RSK (9341, Cell Signaling), goat antibody RSK2 (1430, Santa Cruz), rabbit antibody α-tubulin (4074, Abcam), and mouse antibody α-tubulin (T5168, Sigma). Secondary antibodies were purchased from Jackson laboratories and Abcam.

Mice

NHE1-overexpressing FVB mice were produced by CNRS, SEAT/UPS 44, Villejuif, France. They were generated by transgenesis of a plasmid overexpressing specifically in cardiac muscle cells, a hemagglutinin (HA)-tagged human NHE1, rendered constitutively active by a mutation of the binding domain of calmodulin that normally causes auto inhibition of NHE1 (11). Mice genotyping was performed by standard PCR followed by agarose gel electrophoresis with primers (forward: GAGACCGAGCAGGAGCTCGAG) and (reverse: CAGGTCCACAGACTCGGGTG), for characterizing NHE1 mutant.

OPN-deficient mice ($OPN^{-/-}$) were obtained from Suzan Rittling (Forsyth Institute, Harvard Medical School) and transferred to FVB background. Mice genotyping was performed as previously described using primers (AATATGCGAAGTGGACCTGG) and (GATCAAGCCATAGCCCTTCA) to characterize OPN interruption, and primers (TCCAATGAAAGCCATGACC) and (GAAGAGTGAGTGAATCTGC) to detect WT OPN (29). We produced FVB double transgenic mice expressing mutated NHE1 in $OPN^{-/-}$ and verified genotype by PCR with primers described above.

Mice were handled in the animal facility of INSERM U1034 in accordance with the guidelines established by French Ministry of Agriculture and complying with European Union regulations (license no. B33-318-701). Blinding was achieved by use of a numbering system, whereby each mouse was assigned a specific number, which was not revealed to the individual analyzing the data. The protocol of this project was approved under no. 5012018A by the local Animal Care and Use Committee of Direction Départementale de la Protection des Populations. The Institutional Animal Care and Use Committee at Qatar University, Doha, Qatar, specifically approved this project (Research Ethics Approval Number: QU-IACUC 007/2012).

Western Blot Analysis

Heart tissues were lysed in ice-cold RIPA buffer along with protease inhibitors. Sonication (Branson SLPe) for a few seconds at 20% amplitude facilitated the lysis. Tissue lysates were centrifuged at 12,000 rpm for 15 min at 4°C. The supernatant containing protein was collected and assayed with Bio-Rad DC protein assay kit to determine the concentration. Protein samples (30–40 μg) were denatured by heating at 95°C for 5 min in Laemmli buffer. The samples were then loaded on to SDS polyacrylamide gels. After the run, separated protein samples were transferred on to a nitrocellulose membrane. The membranes were incubated with 5% (wt/vol) nonfat milk or bovine serum albumin, in Tris buffer saline, pH 7.4, with 0.1% Tween 20 for at least 1 h at room temperature. Following the blocking stage, the membranes were incubated overnight at 4°C with primary antibodies, namely, anti-connexin 43, anti-NFAT, anti-pERK, anti-ERK, anti-pRSK, and anti-RSK2. α-Tubulin served as a loading control. The membranes were then incubated with horseradish peroxidase-conjugated secondary antibodies at room temperature for 1 h and 30 min. Visualization of bands was based on enhanced chemiluminescence reaction. Imaging was done by Fluorchem M FM0564 imager and quantification of bands was performed with Scion software.

Reverse Transcription Quantitative PCR

RNAs were isolated by using Tri Reagent (Molecular Research Center), from cardiac muscle that had been snap-frozen in liquid nitrogen and homogenized, as instructed by the manufacturer. For quantitative RT-PCR analysis, total RNA was reverse transcribed with M-MLV reverse transcriptase (Promega) and amplification was performed on a DNA Engine Opticon2 (MJ Research) using B-R SYBER Green SuperMix (Quanta Biosciences). The primers used are shown in Table 1. The relative expression of each mRNA was calculated by the comparative threshold cycle method and normalized to β-actin mRNA expression.

Histology and Immunohistochemistry

The mouse hearts were fixed in methanol and embedded in paraffin. Paraffin blocks were sectioned in to 7 μm sections and dried overnight. The sections were then deparaffinized with xylene and rehydrated, after xylene removal, with alcohol.

Masson's trichrome staining. Sections were dipped successively *1*) 30 s in hematoxylin and washed 5 min in water, *2*) 1 min in acidic fuchsin and washed twice for 2 min in acetified water, *3*) 5 min in

Table 1. *List of primers used in quantitative PCR*

NHE1	
forward	GCCATTGAGCTGGTGGAGAG
reverse	CGGTCTGAAGTCACAGCCTTG
Endogenous NHE1	
forward	GGGGATTTCATCCACCTCGG
reverse	GGGGATCACATGGAAACCTATCT
TIMP4	
forward	TGACACTCAAAAACTGATCCGGTA
reverse	CATAGCAAGTGGTGATTTGGCAG
CTGF	
forward	GACCCAACTATGATGCGAGCC
reverse	TCCCACAGGTCTTAGAACAGG
Integrin-β3	
forward	GGAAGCAGCGCCCAGATCAC
reverse	TTGTCCACGAAGGCCCCAAA
Collagen3A	
forward	CCATTTGGAGAATGTTGTGCAAT
reverse	GGACATGATTCACAGATTCCAGG
Collagen1	
forward	CCCCGGGACTCCTGGACTT
reverse	GCTCCGACACGCCCTCTCTC
MMP2	
forward	TTCGCTCGTTTCCTTCAACC
reverse	ACTGGGCATGATCTGCACAG
PPARα	
forward	GGGTGGTTGAATCGTGAGG
reverse	TGCCTTTTGCCAACAGTAGTAC
PGC1α	
forward	AGACGGATTGCCCTCATTTGA
reverse	TGTAGCTGAGCTGAGTGTTGG
SGK1	
forward	CTGCTCGAAGCACCCTTACC
reverse	TCCTGAGGATGGGACATTTTCA
IL-6	
forward	CACTTCACAAGTCGGAGGCT
reverse	CTGCAAGTGCATCATCGTTGT
OPN	
forward	TCCTATAGCCACATGGCTGG
reverse	CAGAATCCTCGCTCTCTGCA
ANP	
forward	CGTCTTGGCCTTTTGGCTTC
reverse	GGTGGTCTAGCAGGTTCTTGAAA
BNP	
forward	AAGCTGCTGGAGCTGATAAGA
reverse	GTTACAGCCCAAACGACTGAC
CD44	
forward	TGGTGGCACACAGCTTGGGG
reverse	GTCAGCTGCCTCAGTCCGGG
β-Actin	
forward	CCTGAACCCTAAGGCCAACC
reverse	TAGCCCTCGTAGATGGGCAC
cFOS	
forward	CAGCTCCCACCAGTGTCTAC
reverse	TCTGCGCAAAAGTCCTGTGT
CREB	
forward	vACCCCTCCCCAAGCTAGTAT
reverse	GGGCATGCACACGTCTTAAC
STAT3	
forward	TGCTTGGGCATCAATCCTGT
reverse	GAGTAGTTCACACCAGGCCC

phosphomolybdic acid and washed quickly in acetified water, *4*) 2 min in light green stain and washed twice quickly in acetified water. Finally, sections were dehydrated by rapid bath in ethanol and xylene and covered by coverslip with a xylene containing mounting resin.

Picrosirius red staining. Sections were incubated for 1 h in Sirius red solution (1 g Sirius red F3B, Sigma-Aldrich) in 1 l of saturated aqueous solution of picric acid) and then washed twice with acidified water (0.5% acetic acid). Sections were than dehydrated by rapid bath in ethanol and in xylene and covered by coverslip with a xylene containing mounting resin. Observation was done with bright-field microscope (Nikon). Collagen appeared in red on a pale yellow background. Quantitative analysis was performed with Image J software.

Wheat germ hemagglutinin. Wheat germ hemagglutinin (WGA) binds on interstitial matrix. Sections were incubated 1 h in the dark with lectin from triticum vulgaris FITC conjugate (# L4895; Sigma-Aldrich, St. Louis, MO) diluted 1:100 (10 μg/ml) in the required buffer. After three washing steps, the sections were covered by coverslip with a water-soluble antifading mounting medium containing DAPI. Observation was done with fluorescent microscope (Zeiss). FITC appeared in green, and DAPI stained nuclei blue. Axiovision was used for cell area measurement.

Immunohistology. The antigens were retrieved with Ventana CC1 buffer (Tris/EDTA buffer, pH 8) by treating the sections for 4 min at 95°C and then for 12 min at 100°C. The endogenous peroxidase was quenched with 3% H_2O_2 in PBS for 30 min. Heart sections were then blocked with Ab Diluent (ROCHE) for at least 20–30 min in a moist chamber. The sections were then probed with primary antibodies to HA tag, connexin 43 and CD44, in Ab Diluent (ROCHE) for 1 h at 37°C. Biotinylated anti-rabbit IgG secondary antibody (RPN1004V, GE Healthcare) was then added at a dilution of 1:100 in Ab diluent (ROCHE) for 1 h at 37°C. Finally, the 3,3-diaminobenzidine (DAB) kit was used. The nuclei were counterstained with hematoxylin. Images were acquired on NIKON microphot-FXA.

Transthoracic Echocardiography

Mice were lightly anesthetized with 1.5% isoflurane. Echocardiography was performed with Vevo 2100 high-frequency high-resolution ultrasound system (Fujifilm VisualSonics) to measure the lengths of interventricular septum in systole (IVSs), interventricular septum in diastole (IVSd), left ventricular internal diameter in systole (LVIDs), left ventricular internal diameter in diastole (LVIDd), left ventricular posterior wall in systole (LVPWs), left ventricular posterior wall in diastole (LVPWd), ejection fraction (EF), fractional shortening (FS), and volumes of left ventricle in systole (LVs) and in diastole (LVd). The percentage of left ventricular (LV) fractional shortening (% FS) was defined as % FS = [(LVIDd − LVIDs) / LVIDd] * 100.

Statistical Analysis

All values expressed were compared with control ± SE. Student's *t*-test was used to compute differences between groups where a $P < 0.05$ was considered a significant difference. Bonferroni correction was utilized for analyzing multiple samples wherever applicable.

RESULTS

Characteristics of NHE1 Transgenic Mice

To determine the expression of NHE1 mRNA and protein in NHE1 transgenic mice, quantitative PCR, immunohistochemical analysis, and Western blot techniques were used. Figure 1*A* shows an increase in the ratio of endogenous NHE1 mRNA expression to β-actin, when compared with the WT (0.0122 ± 0.0008 WT vs. 0.0137 ± 0.001 NHE1). However, this increase was not significant, whereas the ratio of mutated or exogenous NHE1 mRNA expression to β-actin was significantly increased when compared with the WT (0.85 ± 0.3 NHE1; $P = 0.02$) (Fig. 1*B*). Protein expression of NHE1 was also confirmed by Western blot and immunostaining, where anti-hemagglutinin (HA) tag binds to the HA portion of NHE1 protein (Fig. 1, *C* and *D*).

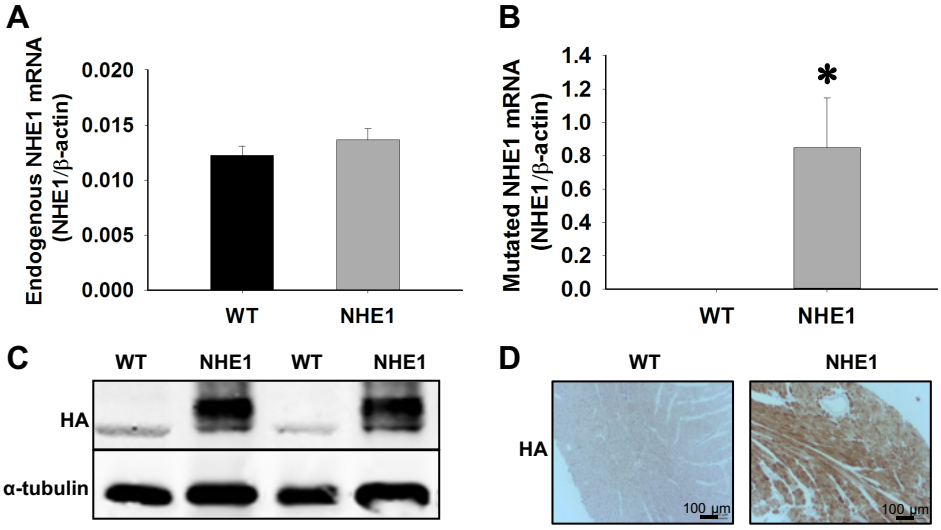

Fig. 1. Na^+/H^+ exchanger isoform 1 (NHE1) mRNA and protein expression in mutated NHE1-overexpressing mice. *A*: RT-quantitative (q)PCR quantification of endogenous NHE1 (eNHE1) mRNA levels in wild-type mice (WT) and NHE1 transgenic mice (NHE1) normalized to β-actin ($n = 7$ for WT and $n = 5$ for NHE1). *B*: RT-qPCR quantification of mutated NHE1 mRNA levels in WT mice and NHE1 transgenic mice (NHE1) normalized to β-actin ($n = 10$ for WT and $n = 9$ for NHE1). Results are expressed as NHE1 mRNA levels ± SE *$P <$ 0.05 vs. WT. *C*: representative Western blot of hemagglutinin (HA) tag demonstrating the comparison of NHE1 protein expression in WT mice and NHE1 transgenic mice. *D*: representative immunohistochemistry images of HA tag demonstrating the comparison of NHE1 protein expression in WT mice and NHE1 transgenic mice.

Heart Overexpression of NHE1 Modulates Extracellular Matrix Degradation, Transcription Factor Expression, Metabolism, and Inflammation of Cardiac Tissue

It is known that NHE1 overexpression induces cardiac hypertrophy. Signaling pathways that mediate this effect have yet to be understood. Quantitative PCR, immunohistochemical staining, and Western blot techniques were used to analyze extracellular matrix (ECM) degradation, transcription factors expression, metabolism, and inflammation. Figure 2*A* demonstrates the modulation of various genes involved in the ECM degradation in NHE1 transgenic mice. Metalloproteinase inhibitor 4 (TIMP4) mRNA expression was significantly reduced in NHE1 transgenic mice when compared with WT (0.0070 ± 0.00060 WT vs. 0.0035 ± 0.0004 NHE1; $P < 0.001$). Connective tissue growth factor (CTGF) (0.2030 ± 0.0306 WT vs. 0.5978 ± 0.1063 NHE1; $P = 0.0057$) and integrin-β3 (0.0005 ± 0.0001 WT vs. 0.0013 ± 0.0003 NHE1; $P = 0.036$) mRNA expression showed a significant increase in NHE1 group compared with the WT. The mRNA expressions of collagen3A (Col3A) (0.0901 ± 0.0151 WT vs. 0.0599 ± 0.0108 NHE1), collagen1 (Col1) (0.0320 ± 0.0049 WT vs. 0.0983 ± 0.0270 NHE1), and matrix metalloproteases 2 (MMP2) (0.0890 ± 0.0073 WT vs. 0.1326 ± 0.0233 NHE1) show no difference between NHE1 and WT groups.

The mRNA expression of transcription factors cFOS (0.0026 ± 0.0008 WT vs. 0.0056 ± 0.0012 NHE1), signal transducer and activator of transcription 3 (STAT3) (0.4624 ± 0.0810 WT vs. 0.5689 ± 0.1553 NHE1), and cyclic adenosine monophosphate response element binding protein (CREB) (0.0050 ± 0.0003 WT vs. 0.0036 ± 0.0008 NHE1) also show no difference between NHE1 and WT (Fig. 2*B*). The mRNA levels of peroxisome proliferator-activated receptor alpha (PPAR-α) and peroxisome proliferator-activated receptor gamma coactivator 1-alpha (PGC-1α) in active NHE1 group are reduced compared with WT group, where the reduction is significant for PPAR-α (0.0494 ± 0.0068 WT vs. 0.0273 ± 0.0032 NHE1; $P =$ 0.017) and PGC-1α (0.1042 ± 0.0153 WT vs. 0.0532 ± 0.0069 NHE1; $P = 0.015$) as demonstrated in Fig. 2*C*. Figure 2*D* demonstrates that gene expression of interleukin 6 (IL-6) has a significant increase in NHE1 group when related to WT ($0.0001 \pm 2.025 \times 10^{-5}$ WT vs. 0.0008 ± 0.0002 NHE1; $P =$ 0.0032). As in agreement with previous data, we have demonstrated that OPN mRNA expression is strongly increased in NHE1 group (0.00072 ± 0.00019 WT vs. 0.0016 ± 0.00017

Fig. 2. Cardiac gene modulation in NHE1-overexpressing mice. Quantification of mRNA levels (*A, B, C, D,* and *F*) was performed by RT-qPCR in wild-type mice (WT) and NHE1 transgenic mice (NHE1) normalized to β-actin. Results are expressed as the ratio of target gene over β-actin ± SE. +$P <$ 0.001 vs. WT, #$P <$ 0.01 vs. WT, *$P <$ 0.05 vs. WT. *A*: quantification of mRNA levels of metalloproteinase inhibitor 4 (TIMP4), connective tissue growth factor (CTGF), integrin-β3 (intβ3), collagen3A (Col3), collagen1 (Col1), and matrix metalloproteases 2 (MMP2). For TIMP4, integrin-β3, collagen3A, collagen1, and MMP2, $n = 7$ for WT and $n = 5$ for NHE1. For CTGF, $n = 10$ for WT and $n = 9$ for NHE1. *B*: quantification of mRNA levels of cFos, cyclic adenosine monophosphate response element binding protein (CREB), signal transducer and activator of transcription 3 (STAT3) ($n = 7$ for WT and $n = 5$ for NHE1). *C*: quantification of mRNA levels of peroxisome proliferator-activated receptor alpha (PPAR-α) and peroxisome proliferator-activated receptor gamma coactivator 1-alpha (PGC-1α) ($n = 7$ for WT and $n = 5$ for NHE1). *D*: quantification of mRNA levels of interleukin 6 (IL-6) ($n = 10$ for WT and $n = 9$ for NHE1). *E*: quantification of OPN mRNA in WT mice, NHE1 transgenic mice, OPN knockout NHE1 transgenic mice (NHE1·$OPN^{-/-}$), and OPN knockout mice ($OPN^{-/-}$) normalized to β-actin ($n = 10$ for WT, $n = 9$ for NHE1, $n = 7$ for NHE1·$OPN^{-/-}$, $n = 10$ for $OPN^{-/-}$). #$P <$ 0.01 vs. WT; ¥$P <$ 0.001 vs. NHE1·$OPN^{-/-}$. *F*: quantification of mRNA levels of serum and glucocorticoid-regulated kinase 1 (SGK1) ($n = 7$ for WT and $n = 5$ for NHE1). *G, H, I*: quantification of protein expression in WT and NHE1 mice was performed by Western blot. Specific protein expression was normalized to α-tubulin. Results are expressed as % of WT ± SE. #$P <$ 0.01 vs. WT, *$P <$ 0.05 vs. WT. *G, top left*: representative Western blot images of connexin 43 protein expression in WT and NHE1. Immunoblotting was against connexin 43 (43 kDa) and α-tubulin (50 kDa). *Bottom left*: representative immunohistochemistry images of connexin 43 protein expression in WT and NHE1. *Right*: quantification of Western blot bands of connexin 43 normalized to α-tubulin ($n = 4$ for WT and $n = 4$ for NHE1). *H, left*: representative Western blot images of nuclear factor of activated T cells (NFAT) protein expression in WT and NHE1. Immunoblotting was against NFAT (160 kDa) and α-tubulin (50 kDa). *Right*: quantification of NFAT protein expression normalized to α-tubulin ($n = 9$ for WT and $n = 7$ for NHE1). *I, left*: representative Western blot images of phosphorylated extracellular signal-regulated kinase (pERK) protein expression in WT and NHE1. Immunoblotting was against pERK (42, 44 kDa) and ERK (42, 44 kDa). *Right*: quantification of pERK protein expression normalized to total ERK ($n = 8$ for WT and $n = 5$ for NHE1).

NHE1; $P = 0.0026$) (Fig. 2*E*). As a control we verified that there is no more OPN expression detected in OPN$^{-/-}$ mice.

Furthermore, the mRNA levels of serum and glucocorticoid-regulated kinase 1 (SGK1) (0.0668 ± 0.0082 WT vs. 0.0416 ± 0.0043 NHE1; $P = 0.024$), protein expression of connexin 43 (100 ± 11.39% WT vs. 22.82 ± 3.04% NHE1; $P = 0.023$), and nuclear factor of activated T cells (NFAT) (100 ± 6.84% WT vs. 47.90 ± 10.08% NHE1; $P = 0.0014$) were also investigated and found to be significantly reduced in the NHE1 group when compared with control (Fig. 2, *F–H*). The NHE1 group also showed a significant increase in phosphorylation of ERK when compared with WT (100 ± 11.97% WT vs. 282.84 ± 50.95% NHE1; $P = 0.021$) (Fig. 2*I*).

Overexpression of NHE1 in the Heart Increases CD 44 Protein Expression through OPN

Immunohistochemistry images of heart sections demonstrate that CD 44 was highly expressed in NHE1 transgenic mice when compared with WT (Fig. 3*A*). This was further confirmed by qPCR (CD 44 mRNA: 0.0047 ± 0.0004 WT vs. 0.0096 ± 0.0010 NHE1; $P < 0.001$) (Fig. 3*B*). Immunostaining and quantitative PCR results also show that the increase in CD 44 expression in NHE1 transgenic mice was inhibited in OPN knockout NHE1 transgenic mice (0.0096 ± 0.0010 NHE1 vs. 0.0057 ± 0.0007 NHE1 OPN$^{-/-}$; $P = 0.0073$), explaining the role of OPN in the expression of CD 44. CD 44 mRNA

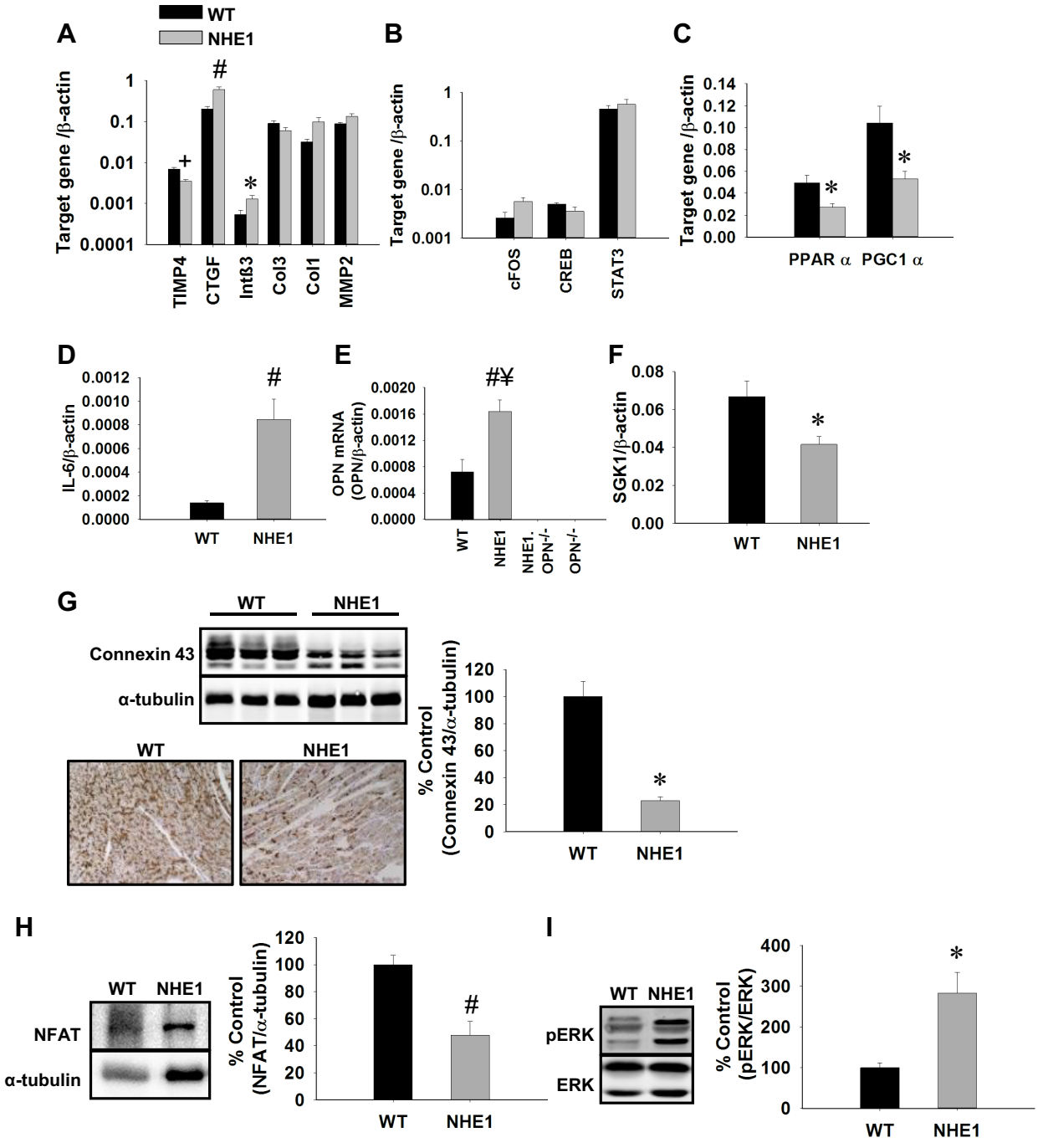

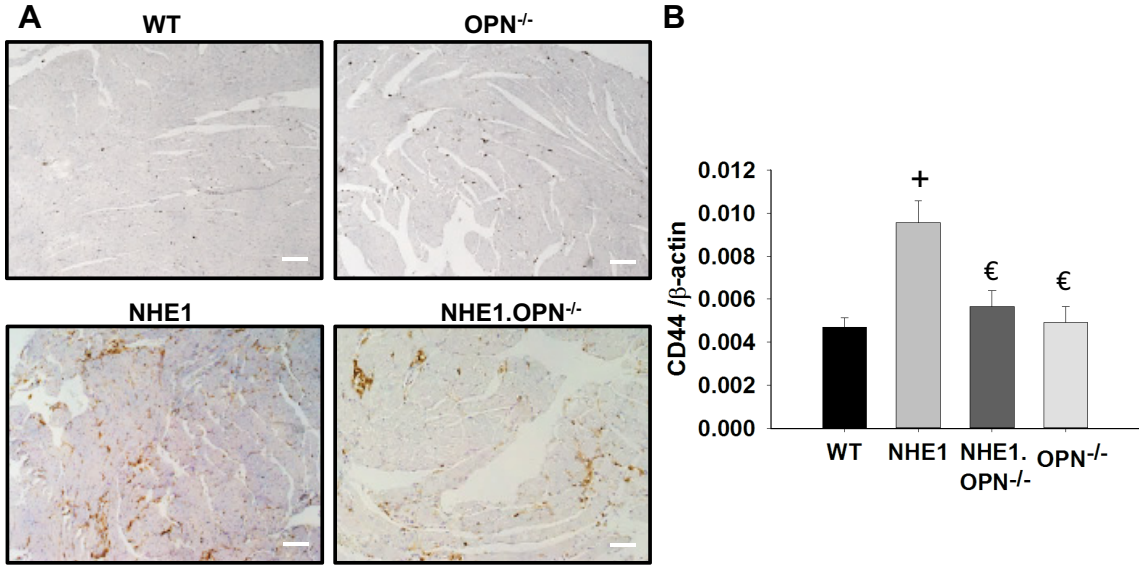

Fig. 3. Role of osteopontin (OPN) in NHE1 overexpression-induced CD44 protein expression. *A*: representative immunohistochemistry images of CD44 expression in the heart cross sections of wild-type mice (WT), NHE1 transgenic mice (NHE1), OPN knockout NHE1 transgenic mice (NHE1·OPN$^{-/-}$), and OPN knockout mice (OPN$^{-/-}$). Bars represent 100 μm. *B*: quantification of mRNA levels of CD 44 normalized to β-actin (n = 10 for WT, n = 9 for NHE1, n = 7 for NHE1·OPN$^{-/-}$, n = 10 for OPN$^{-/-}$). Results are expressed as the ratio of CD44 gene over β-actin ± SE. +$P < 0.001$ vs. WT; €$P < 0.01$ vs. NHE1.

expression was also significantly reduced in OPN$^{-/-}$ mice when compared with NHE1 overexpressed mice (0.0096 ± 0.0010 NHE1 vs. 0.0049 ± 0.00074 OPN$^{-/-}$; P = 0.002).

Heart Overexpression of NHE1 Increases Phosphorylation of p90 Ribosomal S6 Kinase

Western blot image (Fig. 4*A*) and its quantification (Fig. 4*B*) demonstrate that NHE1 transgenic mice showed increased phosphorylation of p90RSK (100 ± 10.21% WT vs. 346.95 ± 82.98% NHE1; P = 0.016), the effect of which was significantly reduced when OPN was knocked out (346.95 ± 82.98% NHE1 vs. 82.17 ± 24.18% NHE1 OPN$^{-/-}$; P = 0.012), indicating the importance of OPN in phosphorylation of RSK. Phosphorylation of RSK was also significantly reduced in OPN$^{-/-}$ mice when compared with NHE1-overexpressed mice (346.95 ± 82.98% NHE1 vs. 134.45 ± 31.54 OPN$^{-/-}$; P = 0.03).

OPN Knockout Regressed Collagen Deposition in NHE1-expressing Transgenic Mice

Cardiac hypertrophic markers including ANP and BNP mRNA expression, cardiac cross-sectional cell area and collagen deposition were assessed to determine the effect of overexpression of NHE1 in the heart. Figure 5*A* depicts an increase in the whole heart size of NHE1 transgenic mice when compared with the WT. Figure 5*B* is Masson's trichrome staining and Fig. 5*E* is Picrosirius red staining of collagen, which showed a significant increase in collagen deposition in the heart cross sections of NHE1 group (2.9 ± 0.28 WT vs. 9.1 ± 0.75 NHE1; $P < 0.001$) and NHE1 OPN$^{-/-}$ group (2.9 ± 0.28 WT vs. 6.2 ± 0.19 NHE1 OPN$^{-/-}$; $P < 0.001$). Figure 5*C* shows that there is a significant increase in the ANP (0.6951 ± 0.18 WT vs. 35.32 ± 5.59 NHE1; $P < 0.001$) and BNP (3.41 ± 0.70 WT vs. 9.19 ± 1.10 NHE1; $P < 0.001$) mRNA expression in the NHE1 transgenic mice. ANP (0.6951 ± 0.18

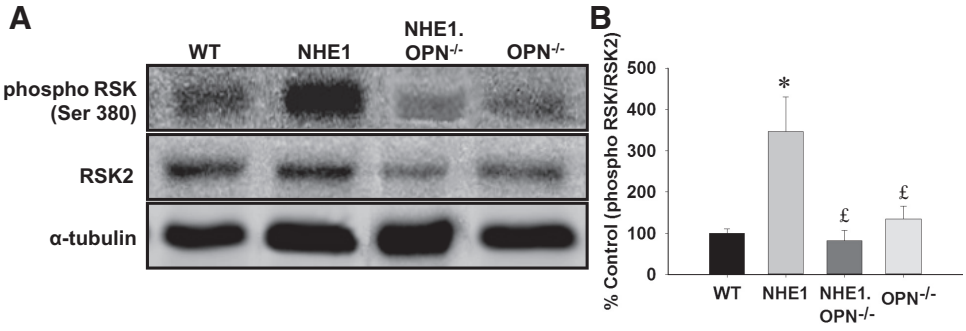

Fig. 4. Role of OPN in NHE1 overexpression-induced phosphorylation of p90 ribosomal S6 kinase. *A*: representative Western blot images of phosphorylated p90RSK protein expression in wild-type mice (WT), NHE1 transgenic mice (NHE1), OPN knockout NHE1 transgenic mice (NHE1·OPN$^{-/-}$), and OPN knockout mice (OPN$^{-/-}$). Immunoblotting was against phospho-p90RSK (90 kDa), RSK2 (80 kDa), and α-tubulin (50 kDa). *B*: quantification of phospho-p90RSK protein expression normalized to RSK2 (n = 7 for WT, n = 7 for NHE1, n = 3 for NHE1·OPN$^{-/-}$, n = 6 for OPN$^{-/-}$). Results are expressed as % of WT ± SE *$P < 0.05$ vs. WT, £$P < 0.05$ vs. NHE1.

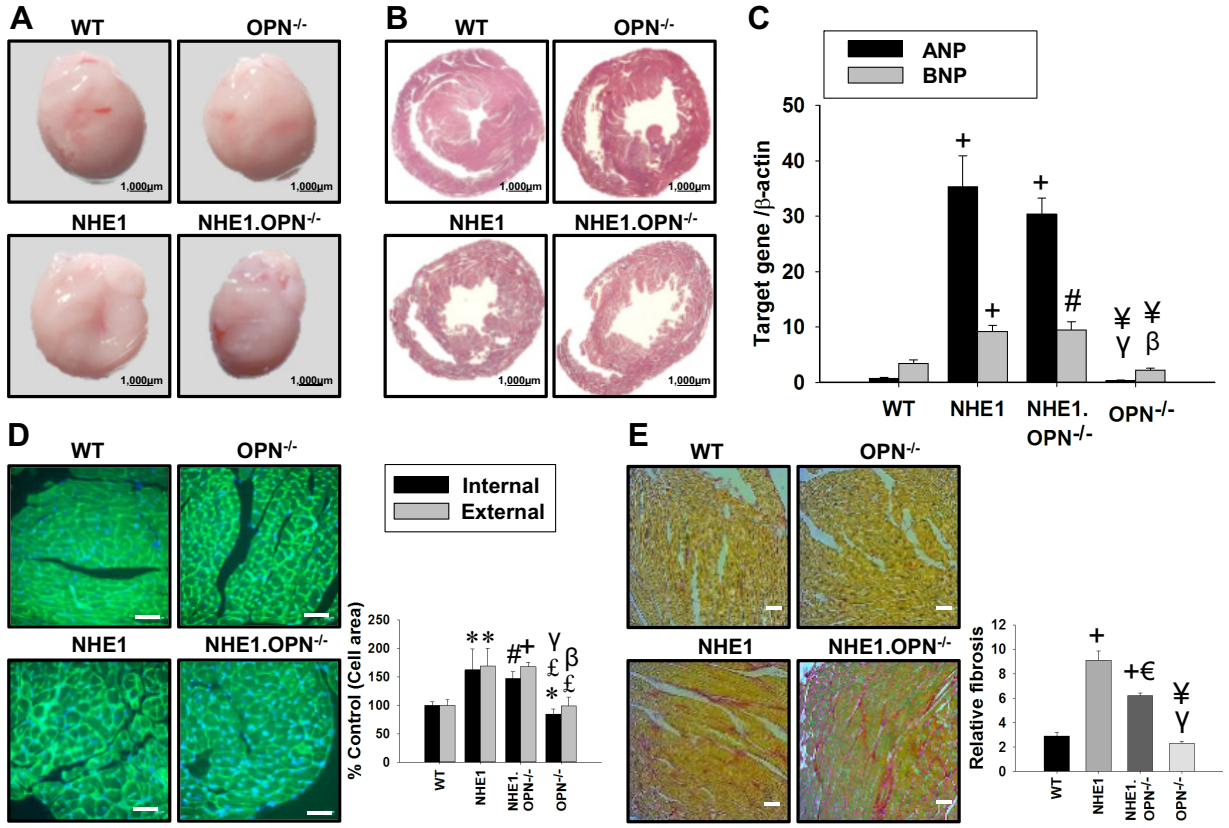

Fig. 5. Role of OPN deficiency and NHE1 overexpression in cardiac morphology. Morphology and histology of heart from wild-type mice (WT), NHE1 transgenic mice (NHE1), OPN knockout NHE1 transgenic mice (NHE1·OPN$^{-/-}$), and OPN knockout mice (OPN$^{-/-}$). *A*: representative whole heart images. *B*: representative images of Masson's trichrome staining of heart cross sections. *C*: quantification of mRNA levels of atrial natriuretic peptide (ANP) and brain natriuretic peptide (BNP) normalized to β-actin (n = 10 for WT, n = 9 for NHE1, n = 7 for NHE1·OPN$^{-/-}$, n = 10 for OPN$^{-/-}$). Results are expressed as the ratio of target gene over β-actin ± SE. +$P < 0.001$ vs. WT, #$P < 0.01$ vs. WT, ¥$P < 0.001$ vs. NHE1, γ$P < 0.001$ vs. NHE1 OPN$^{-/-}$, β$P < 0.01$ vs. NHE1 OPN$^{-/-}$ *D, left* representative images of heart cross sections stained with wheat germ agglutinin (WGA). *Right*: graphical representation of internal and external cross-sectional heart cell area (n = 7 for WT, n = 4 for NHE1, n = 4 for NHE1·OPN$^{-/-}$, n = 4 for OPN$^{-/-}$ for internal cell area; n = 8 for WT, n = 5 for NHE1, n = 3 for NHE1·OPN$^{-/-}$, n = 4 for OPN$^{-/-}$ for external cell area). Bars represent 50 µm. Results are expressed as % of WT ± SE *$P \leq$ 0.05 vs. WT, #$P < 0.01$ vs. WT, +$P < 0.001$ vs. WT, γ$P < 0.001$ vs. NHE1 OPN$^{-/-}$, £$P < 0.05$ vs. NHE1, β$P < 0.01$ vs. NHE1 OPN$^{-/-}$. *E, left* representative images of heart cross sections stained with Picrosirius red (PSR). *Right*: graphical representation of quantification of PSR stain on heart cross sections (n = 14 for WT, n = 10 for NHE1, n = 7 for NHE1·OPN$^{-/-}$, n = 9 for OPN$^{-/-}$). Bars represent 50 µm. Results are expressed as relative fibrosis ± SE. +$P < 0.001$ vs. WT, €$P < 0.01$ vs. NHE1, ¥$P < 0.001$ vs. NHE1, γ$P < 0.001$ vs. NHE1 OPN$^{-/-}$.

WT vs. 30.42 ± 2.84 NHE1 OPN$^{-/-}$; $P < 0.001$) and BNP (3.41 ± 0.70 WT vs. 9.45 ± 1.54 NHE1 OPN$^{-/-}$; P = 0.0067) mRNA expression also showed significant increase in NHE1 OPN$^{-/-}$ when compared with WT. However, both ANP (35.32 ± 5.59 NHE1 vs. 0.35 OPN$^{-/-}$; $P < 0.001$) and BNP (9.19 ± 1.10 NHE1 vs. 2.23 ± 0.32 OPN$^{-/-}$; $P < 0.001$) mRNA expression was significantly reduced in OPN−/− when compared with NHE1 transgenic mice. Areas of cells of the internal part of the heart (100 ± 6.59% WT vs. 162.25 ± 37.01% NHE1; P = 0.051) and of the external part of the heart (100 ± 9.39% WT vs. 169.02 ± 30.75% NHE1; P = 0.021) were measured after WGA staining of heart sections. The NHE1 group showed a significant increase over WT (Fig. 5*D*). The NHE1 OPN$^{-/-}$ also showed significant increase in cell area of internal (100 ± 6.59% WT vs. 147.01 ± 11.64 NHE1 OPN$^{-/-}$; P = 0.0013) and external (100 ± 9.39% WT vs. 167.92 ± 7.44 NHE1 OPN$^{-/-}$; $P < 0.001$) parts of the heart when compared with WT. Moreover, cell areas of internal (162.25 ± 37.01% NHE1 vs. 84.23 ± 9.35% OPN$^{-/-}$; P = 0.026) and external (169.02 ± 30.75% NHE1 vs. 99.35 ± 15.44% OPN$^{-/-}$; P = 0.019) parts of the heart also showed significant reduction in OPN$^{-/-}$ mice when compared with NHE1 transgenic mice. Altogether, our results show that stimulation of NHE1 leads to cardiac hypertrophy, but this increase was not reversed when OPN was knocked out in the presence of NHE1 overexpression. However, there was a decrease in cardiac hypertrophic parameters in OPN$^{-/-}$ when compared with NHE1-overexpressed transgenic mice.

Interestingly, we also show that when NHE1 and NHE1 OPN$^{-/-}$ groups were compared, collagen deposition was significantly reduced when OPN was knocked out in NHE1 transgenic mice (9.1 ± 0.75 NHE1 vs. 6.2 ± 0.19 NHE1 OPN$^{-/-}$; P = 0.0031) (Fig. 5*E*). Moreover, we also show that collagen deposition was significantly reduced in OPN$^{-/-}$ mice when compared with NHE1 transgenic mice (9.1 ± 0.75 NHE1 vs. 2.3 ± 0.18 OPN$^{-/-}$; $P < 0.001$).

Heart Overexpression of NHE1 Degrades Echocardiographic Parameters

To determine the effect of heart overexpression of NHE1 in transgenic mice over WT mice, echocardiography was per-

formed to measure lengths of interventricular septum in systole (IVSs), interventricular septum in diastole (IVSd), left ventricular internal diameter in systole (LVIDs), left ventricular internal diameter in diastole (LVIDd), left ventricular posterior wall in systole (LVPWs), left ventricular posterior wall in diastole (LVPWd), ejection fraction (EF), fractional shortening (FS), and volumes of left ventricle in systole (LVs) and in diastole (LVd). Figure 6, *A* and *C*, respectively, shows that the LVIDs (2.56 ± 0.09 WT vs. 3.42 ± 0.15 NHE1; $P < 0.001$), LVIDd (3.62 ± 0.08 WT vs. 4.08 ± 0.11 NHE1; $P = 0.0043$), LVs (24.09 ± 1.95 WT vs. 49.12 ± 5.30 NHE1; $P = 0.0012$), and LVd (55.70 ± 2.97 WT vs. 74.12 ± 4.94 NHE1; $P = 0.0069$) were significantly increased for NHE1 group compared with WT. Moreover, EF (56.63 ± 2.79 WT vs. 34.95 ± 2.69 NHE1; $P < 0.001$) and FS (29.32 ± 1.96 WT vs. 16.56 ± 1.40 NHE1; $P < 0.001$) of ventricle were significantly reduced in the NHE1 group compared with WT as shown in Fig. 6*B*. However, LVIDs remained significantly increased in NHE1 transgenic mouse even when OPN was knocked out (2.56 ± 0.0854 WT vs. 3.69 ± 0.26 NHE1 $OPN^{-/-}$; $P = 0.0046$) (Fig. 6*A*). Furthermore, EF (56.63 ± 2.79 WT vs. 30.18 ± 4.17; $P < 0.001$) and FS (29.32 ± 1.96 WT vs. 14.18 ± 2.07; $P < 0.001$) were significantly reduced in NHE1 $OPN^{-/-}$ compared with WT (Fig. 6*B*). When we compared the NHE1 group against $OPN^{-/-}$, LVIDs (3.42 ± 0.15 NHE1 vs. 2.31 ± 0.13; $P < 0.001$), LVIDd (4.08 ± 0.11 NHE1 vs. 3.56 ± 0.09 $OPN^{-/-}$; $P = 0.002$), LVs (49.12 ± 5.30 NHE1 vs. 19.21 ± 2.56 $OPN^{-/-}$; $P < 0.001$), and LVd (74.12 ± 4.94 NHE1 vs. 53.52 ± 3.43 $OPN^{-/-}$; $P = 0.0039$) were all significantly reduced in $OPN^{-/-}$ mice. Moreover, EF (34.95 ± 2.69 NHE1 vs. 64.70 ± 3.82 $OPN^{-/-}$; $P < 0.001$) and FS (16.56 ± 1.40 NHE1 vs. 35.45 ± 3.03 $OPN^{-/-}$; $P < 0.001$) were significantly increased in $OPN^{-/-}$ when compared with NHE1 transgenic mice.

DISCUSSION

Cardiac hypertrophy is associated with increased expression of active NHE1 and OPN (10, 43, 44). However, a recent finding demonstrated that plasma OPN level is significantly increased in dilated cardiomyopathy subtype rather than hypertrophic cardiomyopathy, indicating that plasma OPN level is associated with overall heart failure severity (28). Our previous research had demonstrated that OPN is involved as a regulator in NHE1-induced cardiac hypertrophy in vitro (22, 23). Moreover, we had previously described that OPN is increased in cardiomyocytes expressing active NHE1, and this increase is attributed partly by RSK (23). We hypothesized that OPN would be a key regulator and a therapeutic target in NHE1 induced cardiac hypertrophy. To support our hypothesis, we performed experiments on WT mice, NHE1-overexpressing transgenic mice, NHE1-overexpressing OPN knockout mice, and in OPN knockout mice, to delineate the signaling mechanisms involved in NHE1-induced cardiac hypertrophy.

Overexpression of Active NHE1 Induces Cardiac Hypertrophy

We investigated the effects of elevated expression of active NHE1 on the myocardium of mice. Transgenic mice expressing active NHE1 showed significant changes in cardiac hypertrophic parameters including increases in ANP mRNA expression, increases in cell area, and increased

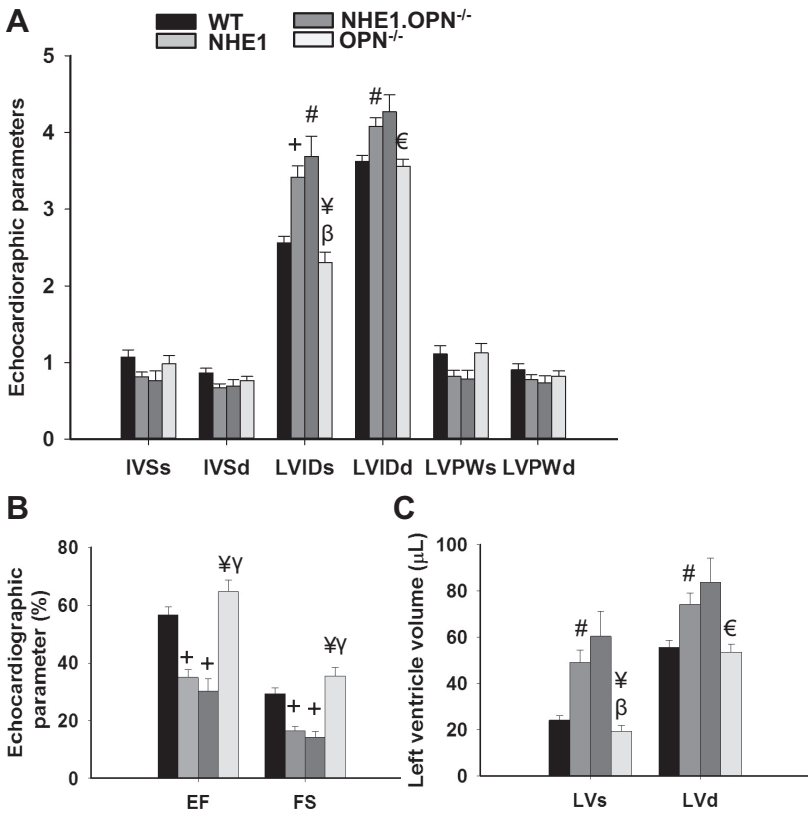

Fig. 6. Effect of NHE1 overexpression on heart function. Graphical representation of echocardiographic parameters of wild-type mice (WT), NHE1 transgenic mice (NHE1), OPN knockout NHE1 transgenic mice (NHE1·$OPN^{-/-}$), and OPN knockout mice ($OPN^{-/-}$). Results are expressed as raw values of echocardiographic parameters ± SE. $+P < 0.001$ vs. WT, $\#P < 0.01$ vs. WT, ¥$P < 0.001$ vs. NHE1, β$P < 0.01$ vs. NHE1 $OPN^{-/-}$, €$P < 0.01$ vs. NHE1, γ$P < 0.001$ vs. NHE1 $OPN^{-/-}$. *A*: graphical representation of the lengths of interventricular septum in systole (IVSs), interventricular septum in diastole (IVSd), left ventricular internal diameter in systole (LVIDs), left ventricular internal diameter in diastole (LVIDd), left ventricular posterior wall in systole (LVPWs), and left ventricular posterior wall in diastole (LVPWd) ($n = 10$ for WT, $n = 9$ for NHE1, $n = 7$ for NHE1·$OPN^{-/-}$, $n = 10$ for $OPN^{-/-}$). *B*: graphical representation of ejection fraction (EF) and fractional shortening (FS) ($n = 10$ for WT, $n = 9$ for NHE1, $n = 7$ for NHE1·$OPN^{-/-}$, $n = 10$ for $OPN^{-/-}$). *C*: graphical representation of volumes of left ventricle in systole (LVs) and diastole (LVd) ($n = 10$ for WT, $n = 9$ for NHE1, $n = 7$ for NHE1·$OPN^{-/-}$, $n = 10$ for $OPN^{-/-}$).

interstitial fibrosis (Fig. 5), which are in accordance with previous reports (24, 44).

Elevated expression and activity of NHE1 also result in cardiac remodeling by regulating matrix metalloproteases (MMPs) and tissue inhibitor of metalloproteases (TIMPs) (44). We observed that expression of TIMP4 was significantly reduced in NHE1-overexpressed transgenic mice, which is in agreement with a previous study that reported decreased TIMP4 in compensatory heart (9). Our results show that PPARα and PGC1α were found to be downregulated in NHE1-overexpressed transgenic mice (Fig. 2*C*), which is in agreement with a previous study performed on failing hearts from patients with dilated cardiomyopathies (30). A previous study demonstrated the role of SGK1 in NHE expression and activity, as well as its involvement in contributing various indices of cardiac hypertrophy including ANP mRNA expression, collagen deposition, and decreased EF finally leading to cardiac remodeling and heart failure (39). Moreover, it has been reported that SGK1 is involved in inflammatory, fibrotic, and oxidative pathways leading to cardiac hypertrophy (19). In contrast, our results demonstrate that NHE1-overexpressed transgenic mice showed a decreased expression of SGK1 (Fig. 2*F*). Previous research indicated that IL-6 mediates cardiac remodeling and cardiac hypertrophy (8, 21, 27), which is in accordance with our study, which showed an upregulation of IL-6 in NHE1-overexpressed transgenic mice (Fig. 2*D*). We show a decrease in connexin 43 protein in NHE1-overexpressed transgenic mice (Fig. 2*G*), in agreement with a previous study that showed decrease in connexin 43 in the presence of high mechanical load leading to hypertrophied myocardium (3). Furthermore, it was reported that NHE1 negatively regulates connexin 43 expression in phenylephrine-induced cardiac hypertrophy (32). Overall, these findings suggest that active NHE1 is sufficient to induce cardiac hypertrophy.

OPN Mediates NHE1-induced Cardiac Hypertrophy through p90 RSK

A previous study also reported that expression of active NHE1 upregulated OPN gene expression significantly (44). Our study confirms that overexpression of NHE1 in the heart upregulated cardiac mRNA expression of OPN, indicating the importance of active NHE1 in expression of OPN. It was previously reported that OPN is a ligand for receptor CD44 (14, 31). Cell adhesion, cell survival, and gene expression were modulated by integrin and CD44-mediated pathways signaled by OPN (7). OPN is susceptible to cleavage at integrin binding motifs (4). Moreover, our results show an increased upregulation of CD44 mRNA and protein expression in transgenic mice overexpressing NHE1, which was reduced when OPN was knocked out in NHE1 transgenic mice (Fig. 3). We are the first to report these findings. Together these findings confirm the correlation that OPN expression is upregulated in heart overexpressing NHE1. Moreover, our previous in vitro study on cardiomyocytes showed that NHE1-induced OPN expression facilitated cardiac hypertrophy as demonstrated by the increase in ANP mRNA expression, cell surface area, and protein content. These markers of hypertrophy were reversed when OPN was downregulated by transfection of siRNA directed against OPN in cardiomyocytes expressing active NHE1 (23). In contrast, in our present in vivo study the increase in ANP mRNA expression and cell surface area in NHE1 transgenic mice was not reversed when OPN was knocked out (Fig. 5*C*). The discrepancy observed with our in vitro (23) findings vs. our in vivo findings may be due to the study model with the former study being carried out in an in vitro cell line, whereas the current study was carried out in an in vivo model. The decrease in cell area and ANP mRNA expression observed in the in vitro model may have been compensated for by external factors in the in vivo model.

Previous reports revealed the involvement of ERK and p90 RSK in mediating cardiac hypertrophy (37). It was also reported that ERK is mediating activation of NHE1 (2, 18). Our results showed increased phosphorylated ERK in overexpressed NHE1 transgenic mice (Fig. 2*I*). Moreover, previous studies reported that RSK is considered to enhance NHE1 activity (34, 36), which is in accordance with our results where active NHE1 transgenic mice showed increased phosphorylation of RSK (Fig. 4). Our novel findings also show that the phosphorylation of RSK was regressed in NHE1 $OPN^{-/-}$ mice (Fig. 4), suggesting that the OPN is a key regulator in the activation of RSK. Furthermore, increased fibrosis in overexpressed NHE1 transgenic mice, which was reduced in NHE1 $OPN^{-/-}$ mice (Fig. 5*E*), also explains the role of OPN in NHE1-induced cardiac hypertrophy.

However, our study also found out that cardiac hypertrophy induced by NHE1 was not reversed when OPN was knocked out in NHE1 transgenic mice, demonstrated in ANP, BNP mRNA expressions and cardiac cell area of NHE1 $OPN^{-/-}$. Moreover, heart function measured by echocardiography was also not improved in NHE1 $OPN^{-/-}$ mice. Furthermore, a significant but not complete reduction in relative fibrosis was observed in NHE1 $OPN^{-/-}$. The partial reduction in cardiac fibrosis may be attributed to the fact that fibrosis may also be caused by other factors including TGF-β (17, 38), accounting for the inability of knocking out OPN for a complete reduction of fibrosis. Together our findings suggest that knocking out OPN only helps in a partial reduction of NHE1-induced cardiac hypertrophy.

Our study also shows no significant changes for cardiac hypertrophic parameters when WT is compared with $OPN^{-/-}$ mice. However, when $OPN^{-/-}$ was compared with NHE1 transgenic mice, we found that the parameters were significantly reduced vs. $OPN^{-/-}$, which could be attributed to the fact that there is no change between WT and $OPN^{-/-}$. This suggests that $OPN^{-/-}$ mice are similar to WT mice, and $OPN^{-/-}$ mice need stimuli like angiotensin, myocardial infarction, or NHE1 overexpression to produce cardiac hypertrophic effects (20).

In conclusion, our findings demonstrate that overexpression of NHE1 results in upregulation of OPN, which ultimately leads to cardiac hypertrophy mediated through CD44 and p90 ribosomal s6 kinase expression.

GRANTS

This work was supported by the National Priorities Research Program grant (NPRP 5 - 330 - 3 - 090) provided by the Qatar National Research Fund, Doha, Qatar (https://www.qnrf.org). Lead principal investigator (PI): FM, PI: LF, AG. "The funders had no role in study design, data collection and analysis, decision to publish, or preparation of the manuscript."

DISCLOSURES

No conflicts of interest, financial or otherwise, are declared by the authors.

AUTHOR CONTRIBUTIONS

N.A., B.J.-V., A.J., S.R., A.-P.G., and F.M. performed experiments; N.A., A.-P.G., and F.M. analyzed data; N.A., B.J.-V., A.-P.G., and F.M. interpreted results of experiments; N.A., A.-P.G., and F.M. prepared figures; N.A. and F.M. drafted manuscript; N.A., L.F., S.R., A.-P.G., and F.M. edited and revised manuscript; N.A., B.J.-V., L.F., A.J., S.R., A.-P.G., and F.M. approved final version of manuscript; A.-P.G. and F.M. conceived and designed research.

REFERENCES

1. **Baartscheer A, Schumacher CA, Wüst RCI, Fiolet JWT, Stienen GJM, Coronel R, Zuurbier CJ.** Empagliflozin decreases myocardial cytoplasmic Na^+ through inhibition of the cardiac Na^+/H^+ exchanger in rats and rabbits. *Diabetologia* 60: 568–573, 2017. doi:10.1007/s00125-016-4134-x.
2. **Bianchini L, L'Allemain G, Pouysségur J.** The p42/p44 mitogen-activated protein kinase cascade is determinant in mediating activation of the Na+/H+ exchanger (NHE1 isoform) in response to growth factors. *J Biol Chem* 272: 271–279, 1997. doi:10.1074/jbc.272.1.271.
3. **Bupha-Intr T, Haizlip KM, Janssen PM.** Temporal changes in expression of connexin 43 after load-induced hypertrophy in vitro. *Am J Physiol Heart Circ Physiol* 296: H806–H814, 2009. doi:10.1152/ajpheart.01058.2008.
4. **Christensen B, Schack L, Kläning E, Sørensen ES.** Osteopontin is cleaved at multiple sites close to its integrin-binding motifs in milk and is a novel substrate for plasmin and cathepsin D. *J Biol Chem* 285: 7929–7937, 2010. doi:10.1074/jbc.M109.075010.
5. **Ennis IL, Escudero EM, Console GM, Camihort G, Dumm CG, Seidler RW, Camilión de Hurtado MC, Cingolani HE.** Regression of isoproterenol-induced cardiac hypertrophy by Na+/H+ exchanger inhibition. *Hypertension* 41: 1324–1329, 2003. doi:10.1161/01.HYP.0000071180.12012.6E.
6. **Fliegel L.** Regulation of the Na(+)/H(+) exchanger in the healthy and diseased myocardium. *Expert Opin Ther Targets* 13: 55–68, 2009. doi:10.1517/14728220802600707.
7. **Frangogiannis NG.** Matricellular proteins in cardiac adaptation and disease. *Physiol Rev* 92: 635–688, 2012. doi:10.1152/physrev.00008.2011.
8. **Fredj S, Bescond J, Louault C, Delwail A, Lecron JC, Potreau D.** Role of interleukin-6 in cardiomyocyte/cardiac fibroblast interactions during myocyte hypertrophy and fibroblast proliferation. *J Cell Physiol* 204: 428–436, 2005. doi:10.1002/jcp.20307.
9. **Givvimani S, Tyagi N, Sen U, Mishra PK, Qipshidze N, Munjal C, Vacek JC, Abe OA, Tyagi SC.** MMP-2/TIMP-2/TIMP-4 versus MMP-9/TIMP-3 in transition from compensatory hypertrophy and angiogenesis to decompensatory heart failure. *Arch Physiol Biochem* 116: 63–72, 2010. doi:10.3109/13813451003652997.
10. **Graf K, Do YS, Ashizawa N, Meehan WP, Giachelli CM, Marboe CC, Fleck E, Hsueh WA.** Myocardial osteopontin expression is associated with left ventricular hypertrophy. *Circulation* 96: 3063–3071, 1997. doi:10.1161/01.CIR.96.9.3063.
11. **Imahashi K, Mraiche F, Steenbergen C, Murphy E, Fliegel L.** Overexpression of the Na+/H+ exchanger and ischemia-reperfusion injury in the myocardium. *Am J Physiol Heart Circ Physiol* 292: H2237–H2247, 2007. doi:10.1152/ajpheart.00855.2006.
12. **Javadov S, Rajapurohitam V, Kilić A, Zeidan A, Choi A, Karmazyn M.** Anti-hypertrophic effect of NHE-1 inhibition involves GSK-3beta-dependent attenuation of mitochondrial dysfunction. *J Mol Cell Cardiol* 46: 998–1007, 2009. doi:10.1016/j.yjmcc.2008.12.023.
13. **Karmazyn M.** NHE-1: still a viable therapeutic target. *J Mol Cell Cardiol* 61: 77–82, 2013. doi:10.1016/j.yjmcc.2013.02.006.
14. **Kazanecki CC, Uzwiak DJ, Denhardt DT.** Control of osteopontin signaling and function by post-translational phosphorylation and protein folding. *J Cell Biochem* 102: 912–924, 2007. doi:10.1002/jcb.21558.
15. **Kehat I, Molkentin JD.** Molecular pathways underlying cardiac remodeling during pathophysiological stimulation. *Circulation* 122: 2727–2735, 2010. doi:10.1161/CIRCULATIONAHA.110.942268.
16. **Lin X, Yang P, Reece EA, Yang P.** Pregestational type 2 diabetes mellitus induces cardiachypertrophy in the murine embryo through cardiacremodeling and fibrosis. *Am J Obstet Gynecol* 217: 216.e1–216.e13, 2017. doi:10.1016/j.ajog.2017.04.008.
17. **Ma F, Li Y, Jia L, Han Y, Cheng J, Li H, Qi Y, Du J.** Macrophage-stimulated cardiac fibroblast production of IL-6 is essential for TGF β/Smad activation and cardiac fibrosis induced by angiotensin II. *PLoS One* 7: e35144, 2012. doi:10.1371/journal.pone.0035144.
18. **Malo ME, Li L, Fliegel L.** Mitogen-activated protein kinase-dependent activation of the Na+/H+ exchanger is mediated through phosphorylation of amino acids Ser770 and Ser771. *J Biol Chem* 282: 6292–6299, 2007. doi:10.1074/jbc.M611073200.
19. **Martín-Fernández B, Valero Muñoz M, de las Heras N, Ballesteros S, Lahera V.** Relevance of SGK1 in structural, functional and molecular alterations produced by aldosterone in heart. *Horm Mol Biol Clin Investig* 18: 53–61, 2014.
20. **Matsui Y, Jia N, Okamoto H, Kon S, Onozuka H, Akino M, Liu L, Morimoto J, Rittling SR, Denhardt D, Kitabatake A, Uede T.** Role of osteopontin in cardiac fibrosis and remodeling in angiotensin II-induced cardiac hypertrophy. *Hypertension* 43: 1195–1201, 2004. doi:10.1161/01.HYP.0000128621.68160.dd.
21. **Meléndez GC, McLarty JL, Levick SP, Du Y, Janicki JS, Brower GL.** Interleukin 6 mediates myocardial fibrosis, concentric hypertrophy, and diastolic dysfunction in rats. *Hypertension* 56: 225–231, 2010. doi:10.1161/HYPERTENSIONAHA.109.148635.
22. **Mlih M, Abdulrahman N, Gadeau A-P, Mohamed IA, Jaballah M, Mraiche F.** Na(+)/H (+) exchanger isoform 1 induced osteopontin expression in cardiomyocytes involves NFAT3/Gata4. *Mol Cell Biochem* 404: 211–220, 2015. doi:10.1007/s11010-015-2380-8.
23. **Mohamed IA, Gadeau AP, Fliegel L, Lopaschuk G, Mlih M, Abdulrahman N, Fillmore N, Mraiche F.** Na+/H+ exchanger isoform 1-induced osteopontin expression facilitates cardiomyocyte hypertrophy. *PLoS One* 10: e0123318, 2015. doi:10.1371/journal.pone.0123318.
24. **Mraiche F, Oka T, Gan XT, Karmazyn M, Fliegel L.** Activated NHE1 is required to induce early cardiac hypertrophy in mice. *Basic Res Cardiol* 106: 603–616, 2011. doi:10.1007/s00395-011-0161-4.
25. **Nolly MB, Pinilla AO, Ennis IL, Cingolani HE, Morgan PE.** Cardiac hypertrophy reduction in SHR by specific silencing of myocardial Na(+)/H(+) exchanger. *J Appl Physiol* 118: 1154–1160, 2015. doi:10.1152/japplphysiol.00996.2014.
26. **Oka T, Akazawa H, Naito AT, Komuro I.** Angiogenesis and cardiac hypertrophy: maintenance of cardiac function and causative roles in heart failure. *Circ Res* 114: 565–571, 2014. doi:10.1161/CIRCRESAHA.114.300507.
27. **Papay RS, Shi T, Piascik MT, Naga Prasad SV, Perez DM.** α_1A-adrenergic receptors regulate cardiac hypertrophy in vivo through interleukin-6 secretion. *Mol Pharmacol* 83: 939–948, 2013. doi:10.1124/mol.112.084483.
28. **Podzimkova J, Palecek T, Kuchynka P, Marek J, Danek BA, Jachymova M, Kalousova M, Zima T, Linhart A.** Plasma osteopontin levels in patients with dilated and hypertrophic cardiomyopathy. *Herz* 16 Nov: 1–17, 2017. doi:10.1007/s00059-017-4645-3.
29. **Rittling SR, Matsumoto HN, McKee MD, Nanci A, An XR, Novick KE, Kowalski AJ, Noda M, Denhardt DT.** Mice lacking osteopontin show normal development and bone structure but display altered osteoclast formation in vitro. *J Bone Miner Res* 13: 1101–1111, 1998. doi:10.1359/jbmr.1998.13.7.1101.
30. **Sebastiani M, Giordano C, Nediani C, Travaglini C, Borchi E, Zani M, Feccia M, Mancini M, Petrozza V, Cossarizza A, Gallo P, Taylor RW, d'Amati G.** Induction of mitochondrial biogenesis is a maladaptive mechanism in mitochondrial cardiomyopathies. *J Am Coll Cardiol* 50: 1362–1369, 2007. doi:10.1016/j.jacc.2007.06.035.
31. **Senbanjo LT, Chellaiah MA.** CD44: A Multifunctional Cell Surface Adhesion Receptor Is a Regulator of Progression and Metastasis of Cancer Cells. *Front Cell Dev Biol* 5: 18, 2017. doi:10.3389/fcell.2017.00018.
32. **Stanbouly S, Kirshenbaum LA, Jones DL, Karmazyn M.** Sodium hydrogen exchange 1 (NHE-1) regulates connexin 43 expression in cardiomyocytes via reverse mode sodium calcium exchange and c-Jun NH2-terminal kinase-dependent pathways. *J Pharmacol Exp Ther* 327: 105–113, 2008. doi:10.1124/jpet.108.140228.
33. **Sun H, Gao C, Wang Y.** A H(a)rd Way to Adapt in Cardiac Hypertrophy. *Circ Res* 117: 484–486, 2015. doi:10.1161/CIRCRESAHA.115.307164.
34. **Takahashi E, Abe J, Berk BC.** Angiotensin II stimulates p90rsk in vascular smooth muscle cells. A potential Na(+)-H+ exchanger kinase. *Circ Res* 81: 268–273, 1997. doi:10.1161/01.RES.81.2.268.
36. **Takahashi E, Abe J, Gallis B, Aebersold R, Spring DJ, Krebs EG, Berk BC.** p90(RSK) is a serum-stimulated Na+/H+ exchanger isoform-1 kinase. Regulatory phosphorylation of serine 703 of Na+/H+ exchanger isoform-1. *J Biol Chem* 274: 20206–20214, 1999. doi:10.1074/jbc.274.29.20206.
37. **Takeishi Y, Huang Q, Abe J, Glassman M, Che W, Lee JD, Kawakatsu H, Lawrence EG, Hoit BD, Berk BC, Walsh RA.** Src and multiple MAP kinase activation in cardiac hypertrophy and congestive

heart failure under chronic pressure-overload: comparison with acute mechanical stretch. *J Mol Cell Cardiol* 33: 1637–1648, 2001. doi:10.1006/jmcc.2001.1427.

38. **Teekakirikul P, Eminaga S, Toka O, Alcalai R, Wang L, Wakimoto H, Nayor M, Konno T, Gorham JM, Wolf CM, Kim JB, Schmitt JP, Molkentin JD, Norris RA, Tager AM, Hoffman SR, Markwald RR, Seidman CE, Seidman JG.** Cardiac fibrosis in mice with hypertrophic cardiomyopathy is mediated by non-myocyte proliferation and requires Tgf-β. *J Clin Invest* 120: 3520–3529, 2010. doi:10.1172/JCI42028.
39. **Voelkl J, Lin Y, Alesutan I, Ahmed MSE, Pasham V, Mia S, Gu S, Feger M, Saxena A, Metzler B, Kuhl D, Pichler BJ, Lang F.** Sgk1 sensitivity of Na(+)/H(+) exchanger activity and cardiac remodeling following pressure overload. *Basic Res Cardiol* 107: 236, 2012. doi:10.1007/s00395-011-0236-2.
40. **Voelkl J, Pasham V, Ahmed MSE, Walker B, Szteyn K, Kuhl D, Metzler B, Alesutan I, Lang F.** Sgk1-dependent stimulation of cardiac Na+/H+ exchanger Nhe1 by dexamethasone. *Cell Physiol Biochem* 32: 25–38, 2013. doi:10.1159/000350120.
41. **Waller AH, Sanchez-Ross M, Kaluski E, Klapholz M.** Osteopontin in cardiovascular disease: a potential therapeutic target. *Cardiol Rev* 18: 125–131, 2010. doi:10.1097/CRD.0b013e3181cfb646.
42. **Benjamin EJ, Blaha MJ, Chiuve SE, Cushman M, Das SR, Deo R, de Ferranti SD, Floyd J, Fornage M, Gillespie C, Isasi CR, Jiménez MC, Jordan LC, Judd SE, Lackland D, Lichtman JH, Lisabeth L, Liu S, Longenecker CT, Mackey RH, Matsushita K, Mozaffarian D, Mussolino ME, Nasir K, Neumar RW, Palaniappan L, Pandey DK, Thiagarajan RR, Reeves MJ, Ritchey M, Rodriguez CJ, Roth GA, Rosamond WD, Sasson C, Towfighi A, Tsao CW, Turner MB, Virani SS, Voeks JH, Willey JZ, Wilkins JT, Wu JH, Alger HM, Wong SS, Muntner P; American Heart Association Statistics Committee and Stroke Statistics Subcommittee.** Heart Disease and Stroke Statistics-2017 Update: A Report From the American Heart Association. *Circulation* 135: e146–e603, 2017. doi:10.1161/CIR.0000000000000485.
43. **Xie Z, Singh M, Singh K.** Osteopontin modulates myocardial hypertrophy in response to chronic pressure overload in mice. *Hypertension* 44: 826–831, 2004. doi:10.1161/01.HYP.0000148458.03202.48.
44. **Xue J, Mraiche F, Zhou D, Karmazyn M, Oka T, Fliegel L, Haddad GG.** Elevated myocardial Na+/H+ exchanger isoform 1 activity elicits gene expression that leads to cardiac hypertrophy. *Physiol Genomics* 42: 374–383, 2010. doi:10.1152/physiolgenomics.00064.2010.